Computers and Concrete, Vol. 11, No. 4 (2013) 317-336
DOI: http://dx.doi.org/10.12989/cac.2013.11.4.317

Realistic pore structure of Portland cement paste: experimental study and numerical simulation

Hongyan Ma and Zongjin Li*

Department of Civil and Environmental Engineering, the Hong Kong University of Science and Technology, Hong Kong, China

(Received July 4, 2011, Revised August 25, 2012, Accepted October 8, 2012)

Abstract. In this study, the pore structure of Portland cement paste is experimentally characterized by MIP (mercury intrusion porosimetry) and nitrogen adsorption, and simulated by a newly developed status-oriented computer model. Cement pastes with w/c=0.3, 0.4 and 0.5 at ages from 1 day to 120 days are comprehensively investigated. It is found that MIP cannot generate valid pore size distribution curves for cement paste. Nevertheless, nitrogen adsorption can give much more realistic pore size distribution curves of small capillary pores, and these curves follow the same distribution mode. While, large capillary pores can be effectively characterized by the newly developed computer model, and the validity of this model has been proved by BSE imaging plus image analysis. Based on the experimental findings and numerical simulation, a hypothesis is proposed to explain the formation mechanism of the capillary pore system, and the realistic representation of the pore structure of hydrated cement paste is established.

Keywords: cement paste; pore structure; MIP; nitrogen adsorption; computer model

1. Introduction

Cement based materials, such as cement paste, mortar and concrete, are porous materials. The properties of porous materials are strongly affected by the characteristics of their pore system, such as porosity, pore size distribution, connectivity, etc. Thus, materials with the same total pore volume (porosity) may exhibit quite different mechanical and transport properties. In cement based materials, compressive strength and elasticity primarily depend on the porosity (Neville 1996), while transport properties, such as permeability and diffusivity, are influenced by the total volume, size distribution, shape and connectivity of the pores (Aligizaki 2006). Therefore, transport properties of cement based materials have to be studied in strong relationship with the pore structure (Gallé 2001).

In the present paper, the pore structure of cement paste, the matrix and binder phase of concrete, is comprehensively studied using several techniques, as the foundation of modeling transport properties. A general classification of pores in solids according to their average width, say, the diameter of a cylindrical pore or the distance between the sides of a slit-shaped pore, has been frequently quoted in the literature (Aligizaki 2006, Brandt 2009, Webb *et al*. 1997). In this

*Corresponding author, Professor, E-mail: zongjin@ust.hk

Table 1 Chemical composition (%) of cement

SiO_2	Al_2O_3	Fe_2O_3	CaO	MgO	SO_3	Loss on ignition
21.1	5.6	3.4	65.3	1.6	2.1	0.85

Table 2 Physical properties of cement

Specific gravity	Blain specific surface area (cm^2/g)	Setting time (min)		Compressive strength (MPa)		
		Initial	Final	2 days	7 days	28 days
3.15	3580	150	180	24.1	40.7	56.9

classification, pores are categorized into micropores, mesopores and macropores, and concrete scientists usually choose 2.5 nm and 100 nm as the boundaries (Young *et al.* 1998). More generally in concrete science and technology, the pores are distinguished in terms of gel pores, capillary pores, entrained air and entrapped air (CEB 1991). In this study, only capillary pores from several nanometers to tens of micrometers are considered because of their dominate role on transport properties at micro-scale, while gel pores are considered as a part of hydration products, and entrapped air is neglected. For experimental study, the pore structure of cement paste with varying *w/c* (water to cement ratio in mass) and ages are measured by MIP (mercury intrusion porosimetry) and nitrogen adsorption methods. Large capillary pores out of the measuring capacity of nitrogen adsorption are characterized by numerical simulation based on a status-oriented sphere assemblage model, coupled with image analysis. Based on comprehensive comparison and discussion, the realistic pore structure of cement paste is revealed.

2. Materials and experiments

For the experimental studies, only cement pastes were considered, and no mineral additives, chemical admixtures or aggregates were incorporated. Portland cement that satisfies the requirements of BS EN197-1:2000 for CEM I Portland cement of strength class 52.5 N (roughly equivalent to the requirements of ASTM C150 for Type I Portland cement) was used in this study. The chemical compositions and physical properties of the cement are listed in Tables 1 and 2, respectively. Ordinary tap water was used as mixing water of cement paste.

Cement pastes with *w/c* of 0.3, 0.4 and 0.5 were mixed, casted into steel moulds, and sealed by plastic sheet to prevent specimens from water evaporation. After 24 hours, specimens were demoulded and cured in a moisture room where the temperature and relative humidity were approximately 27ºC and higher than 95% respectively. At the curing age of 1, 3, 7, 28, 60 and 120 days, paste specimens were taken out of the curing room. Their near-surface portions were eliminated by a diamond saw, and the left portions was sampled according to the requirements of different tests.

For MIP tests, cuboids with the smallest dimension of 5-8 mm were sawed as samples from the left portion of the specimens as mentioned in the last paragraph, which was followed by a solvent (ethanol) replacement drying procedure suggested by Aligizaki (2006). Based on general suggestions in the literature (Kaufmann *et al.* 2009, Tang 2010, Webb *et al.* 1997, Zhang 2008), in the theoretical calculation of pore diameter by the well-known Washburn equation, the contact

angle between mercury and hardened cement paste was chosen as 130º, while the surface tension of mercury 480 *mN/m*. A Micromeritics AutoPore IV 9500 was used for MIP tests, and the maximum pressure that could be applied is 30500 psi (210 MPa), which approximately corresponds to a minimum detectable pore diameter of 6 nm. For nitrogen adsorption, samples the same as in MIP tests were crushed, pestled and sieved, and small particles ranging from 300 μm to 600 μm were collected for measurements. Nitrogen adsorption isotherms were measured by a Beckman Coulter SA3100 Surface Area and Pore Size Analyzer. Based on Kelvin equation and t-plot, the famous BJH method (Barrett *et al.* 1951) was employed to deduce the pore size distribution curves.

The degree of hydration is a very important input-factor in the microstructure simulation of cement pastes. In this study, it was determined by the classical TGA (thermo-gravimetric analysis) method. Samples were the same as those used for nitrogen adsorption. In a thermal analysis, about 30 mg sample was put in an alumina top-opened crucible and followed by a two-step heating process. In step 1, the temperature was increased from the room temperature to 100ºC, and held for 10 minutes to eliminate the evaporable water. In step 2, the sample was continuously heated from 100ºC to 1000ºC with a heating rate of 10ºC/min. The weight loss data were collected. Nitrogen gas was chosen as the dynamic atmosphere, and corundum the reference material. The degree of hydration was calculated through Eq. (1)

$$\alpha = \frac{W_l}{W_i W_t} \times 100\% \tag{1}$$

where W_l is the total weight loss percentage of sample from 100ºC to 1000ºC; W_i is the remain weight percentage of sample after heating at 1000ºC; W_t is the theoretical weight of chemically bonded water for fully hydrated 1 g of cement (W_t=0.23 g/g); the neglectable influence of the loss on ignition of cement was not considered. Hydration of cement does not produce calcium carbonate, so the carbonation of calcium hydroxide influences the accuracy of this equation. Thus, W_l in Eq. (1) should be corrected by the weight loss percentage due to the decomposition of calcium carbonate, $W_l^{CO_2}$. Determination of $W_l^{CO_2}$ through a TG curve is handy in cement chemistry. With $W_l^{CO_2}$, W_l can be corrected by transforming the weight loss due to the decomposition of calcium carbonate into that of calcium hydroxide, through Eq. (2)

$$W_l = W_l^{'} - W_l^{CO_2}\left(1 - \frac{W_{H_2O}}{W_{CO_2}}\right) = W_l^{'} - 0.59 W_l^{CO_2} \tag{2}$$

where $W_l^{'}$ is the weight loss percentage calculated from the original data; W_{H_2O} and W_{CO_2} are the molecular weight of water and carbon dioxide respectively.

Any numerical simulation needs to be validated theoretically or experimentally. In this study, this was done by BSE (backscattered scanning electron microscopy) imaging coupled with image analysis. For BSE imaging, samples the same as those used for MIP were impregnated with low viscosity epoxy. After that, a surface for imaging was cut by a saw, and further polished following

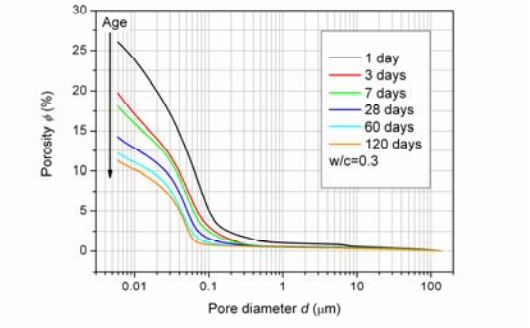

(a) Portland cement paste, *w/c*=0.3

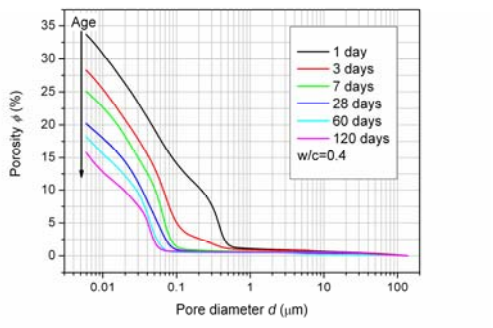

(b) Portland cement paste, *w/c*=0.4

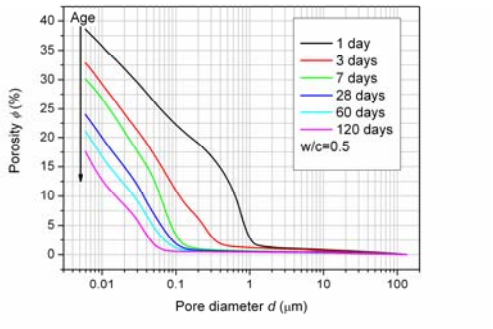

(c) Portland cement paste, *w/c*=0.5

Fig. 1 Cumulative porosity (pore size distribution) curves of Portland cement pastes determined by MIP

the procedure used by Miller *et al.* (2008). Imaging was performed by a JEOL JSM-6390 Scanning Electron Microscope equipped with a backscatter electron detector. BSE images were acquired at a magnification of 500×. Image analysis was carried out by an algorithm developed from the closing operation described by Gonzalez and Woods (2002), to generate the corresponding pore size distribution curve. The same method was also used to analyze the 2D images from computer simulation.

3. Experimental results

3.1 Results of MIP measurements

Cumulative porosity curves of cement paste with *w/c* equal to 0.3, 0.4 and 0.5 are shown in Fig. 1. Each curve is from an average of two measurements. Diamond (2000), the pioneer of applying MIP technique in concrete technology, indicated that the conditions necessary for valid MIP measurements could not be satisfied in cement based materials, and MIP results were valuable only to provide intrudable porosities and threshold diameters which could serve as porosity index and connectivity index respectively for cement based materials (Diamond 2000, Diamond and Leeman 1995). As shown in Fig. 1, porosity and threshold pore diameter vary in large ranges and depend on *w/c* and curing time (age). Longer curing time, as well as lower *w/c*, results in lower

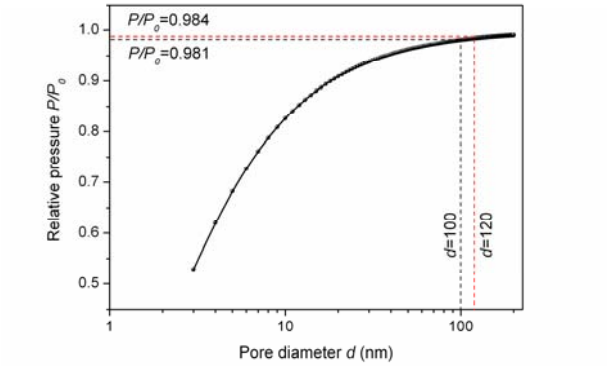

Fig. 2 Relation between pore diameter and corresponding relative pressure

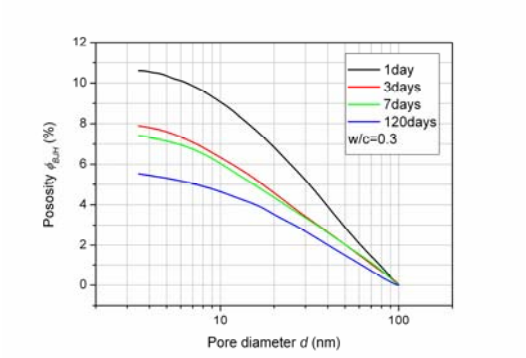

(a) Portland cement paste, *w/c*=0.3

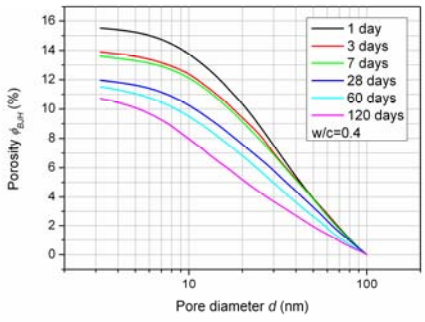

(b) Portland cement paste, *w/c*=0.4

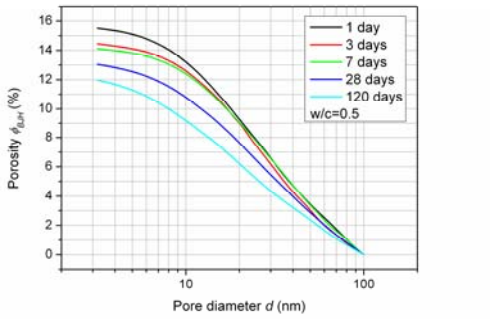

(c) Portland cement paste, *w/c*=0.5

Fig. 3 Cumulative porosity (pore size distribution) curves of Portland cement pastes determined by nitrogen adsorption

porosity and smaller threshold pore diameter. Comparing with Cook and Hover's results (Cook and Hover 1999), which was deservedly considered as an extensive library of MIP curves (Diamond 2000), the intrudable porosity values in Fig. 1 are lower without exception, because the maximum pressure used in the present study is only half of that used by Cook and Hover. More or

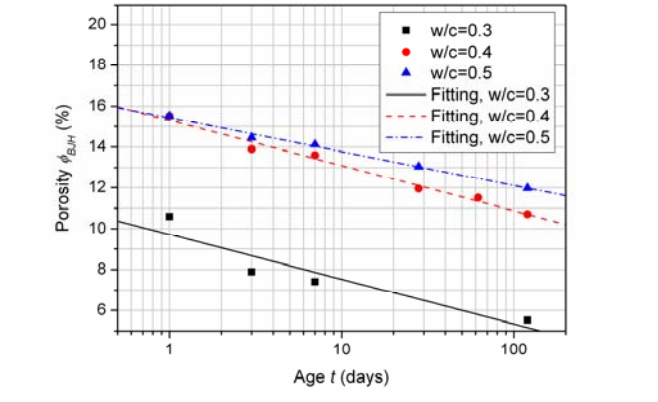

Fig. 4 Influence of *w/c* and age (t in days) on ϕ_{BJH}

less, the higher curing temperature in this study may contribute to the difference. However, the threshold pore diameters agree much better with Cook and Hover's results.

3.2 Results of nitrogen adsorption

3.2.1 Effective range of the method

In BJH method, pore sizes are calculated according to Kelvin equation and Halsey equation (*t*-curve). For micro-pores that the size of the pore is comparable to the size of the gas molecule, the filling mechanism is different from condensation and is known as micro-pore filling. For very large pores, the relative pressure required by condensation is too high to be reached due to experimental or instrumental limitations. Using instruments of present generation, pores can be characterized up to 190 nm in diameter (Aligizaki 2006). However, when the size of pores varies between 100 and 120 nm, the relative pressure needs to vary between 0.981 and 0.984 to detect them (Fig. 2). It is difficult for an instrument to distinguish the pressure difference sensitively in such a small range, thus accuracy cannot be guaranteed. Evidently, the pore size (diameter) that can be characterized by this method is limited in a narrow range, which is from 0.3 nm to 300 nm according to Gerhardt (1989), and from 2 nm to about 120 nm according to Aligizaki (2006) in cement paste. While, 3-100 nm is adopted in the present study, considering both the capacity of instrument and the reason presented above.

3.2.2 Cumulative porosity curves

The pore volume data with unit of $length^3/mass$ generated by BJH method can be easily transformed to porosity data with unit of volume percentage (%). Cumulative porosity (pore size distribution) curves of cement paste with *w/c*=0.3, 0.4 and 0.5, and varying ages, are shown in Fig. 3. In these figures, it can be seen that porosity detected by nitrogen adsorption (ϕ_{BJH}) also decreases as *w/c* decreases, or curing time (or age t) increases. The relationship between ϕ_{BJH}, *w/c*, and t is shown in Fig. 4.

For each *w/c*, the varying of ϕ_{BJH} following the age could be fitted by a linear equation in

log-domain

$$\phi_{BJH} = A - B \times \log_{10}(t) \tag{3}$$

where A and B are constants. For w/c=0.3, A=9.72, B=2.19 and R^2=0.8621; for w/c=0.4, A=15.30, B=2.21 and R^2=0.9806; for w/c=0.5, A=15.43, B=1.66 and R^2=0.9887.

Normalizing the curves in Fig. 3 by dividing each pore size distribution by its highest value ϕ_{BJH}, the normalized cumulative porosity curves can be deduced and plotted in Fig. 5. It is obvious that almost all the curves have very similar shape, which suggests the same distribution mode. Thus, these curves can be unified by one curve without large error. A simple sigmoidal function is selected for the fitting

$$N_{BJH}(d) = \frac{N_1 - N_2}{1 + \left(\frac{d}{d_{mean}}\right)^n} + N_2 \quad , \quad d \in [3, 100] \tag{4}$$

where $N_{BJH}(d)$ is the normalized cumulative porosity which is the function of d, d is pore diameter in *nm*, d_{mean} is the mean pore diameter, n is the exponent, N_1 and N_2 are constants. According to the fitting result, d_{mean}=32.0103 nm, n=1.3352, N_1=1.0667, $N_2 = -0.2249$ and R^2=0.9814.

In this way, combining Eqs. (3) and (4), the pore size distribution curves measured by nitrogen adsorption (PSD_{BJH}) can be unified by the mathematic form

$$PSD_{BJH}(w/c, t, d) = \phi_{BJH}(w/c, t) \cdot N_{BJH}(d), \quad d \in [3, 100] \tag{5}$$

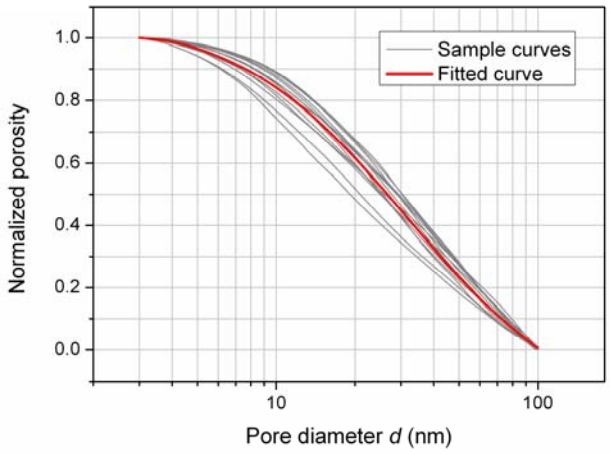

Fig. 5 Normalized cumulative porosity curves and the unified curve

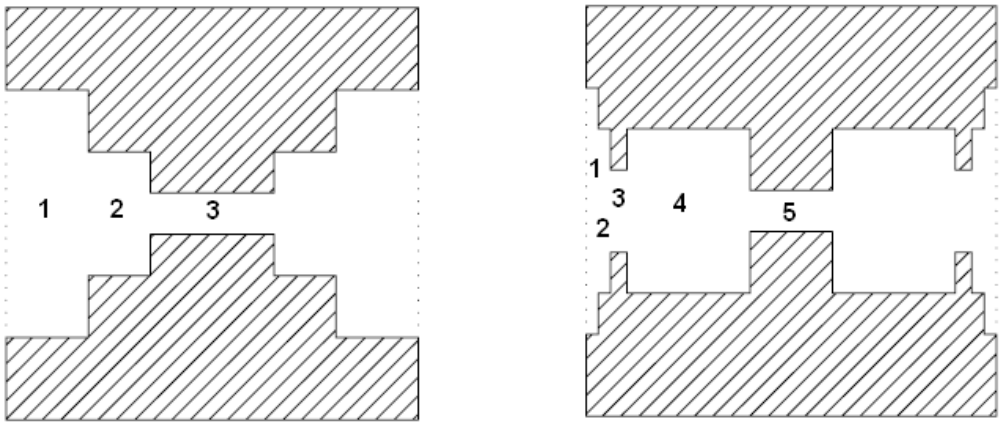

(a) A sample suitable for MIP (b) A sample unsuitable for MIP

Fig. 6 Sketches of samples suitable and unsuitable for MIP measurements to give valid pore size distribution

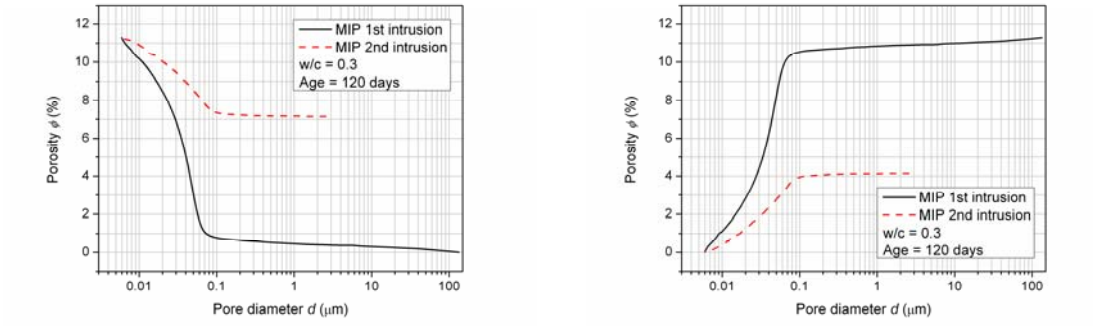

(a) Curves directly from MIP output file (b) Re-plotted curves

Fig. 7 Pore size distribution curves generated from MIP 1st and 2nd intrusion

3.3 Comparison of MIP and nitrogen adsorption results

3.3.1 Intrinsic drawbacks of MIP

MIP technique has intrinsic drawbacks that are difficult to be overcome. It is manifested in two aspects. On one hand, the uncertainty of the contact angle between mercury and the pore wall makes it difficult to get the true pore size. On the other hand, the ink-bottle effect of the pore system makes it impossible to deduce the true volume of pores with each size (Diamond 2000). Considering the former, a large range of the contact angle can be found in literature, from 117º to 141º, which results in differences in pore size by a factor up to 2 (Cook and Hover 1991, 1999, Winslow and Diamond 1970, Moro and Böhni 2002). Winslow and Diamond (1970) even suggested different contact angles for samples dried by different methods, say, 130º for P-drying, 126º for D-drying and 117º for oven drying. However, it is not true that many adopt these values, more researchers preferred to select a unique value, say, 130º for all measurements (Cook and Hover 1999, Kaufmann *et al.* 2009, Webb *et al.* 1997, Zhang 2008). If all researchers adopt similar drying method and the same contact angle, it can be assumed that the contact angle does not lead

to large error. It must be noted that a much smaller value should be selected for the analysis of MIP extrusion process (Kaufmann *et al.* 2009, León 1998). Compared with the former, the later, or the ink-bottle effect is impossible to be overcome, which can be seen in Fig. 6. Fig. 6(a) shows a sample in which the conditions that must be met for MIP measurements can be satisfied. In this sample, mercury can be intruded step by step, from outer larger pores to inner smaller pores, following the increasing of pressure, to provide valid estimates for pore size distribution. The sample shown in Fig. 6(b) can not satisfy the conditions. In this sample, mercury will not enter pore 4, which is the same as pore 2 in diameter, until the pressure corresponding to the size of pore 3, which is smaller than pore 2 and pore 4, thus the volume of pore 4 is added on that of pore 3 rather than itself. In this way, a valid porosity but finer pore structure is generated by MIP. In cement paste, the pore system is much more complex than the sample shown in Fig. 6(b) undoubtedly, and most of the pores are generally reported one or two orders of magnitude smaller than they actually are. Thus MIP can only generate a much finer, rather than the realistic, or even approximate pore structure of cement based materials.

The pore size distribution curve generated by MIP can be adjusted, to some extent, by performing a 2nd intrusion process. The mechanism of the differences between MIP 1st intrusion, 2nd intrusion and nitrogen adsorption has been demonstrated by Kaufmann *et al.* (2009) using a simplified model. After the extrusion process, mercury in ink-bottle pores still stays inside. Thus during the second intrusion, ink-bottle pores (or cavities) will be not available, and only the non-ink-bottle pores (or throats) can be detected from outer larger ones to inner smaller ones, just like the case in Fig. 6(a). Excluding all ink-bottle pores, the 2nd intrusion underestimates the volume of pores of almost all sizes. In Fig. 7, MIP results of cement paste with *w/c*=0.3 at the age of 120 days are plotted for the 1st and 2nd intrusions. Fig. 7(a) is directly plotted from the cumulative pore volume table in a MIP output file, and the start point of the 2nd intrusion curve is the end of an extrusion curve rather than zero. To make the comparison clearer, the incremental pore volume data can be used to re-plot the two curves and make their porosity cumulated from small size to large size. The re-plotted curves are shown in Fig. 7(b). It is thence easy to deduce that the realistic pore size distribution curve should lie between the two curves in Fig. 7(b). Besides, as very large amount of capillary pores lager than the threshold pore size exist, which can

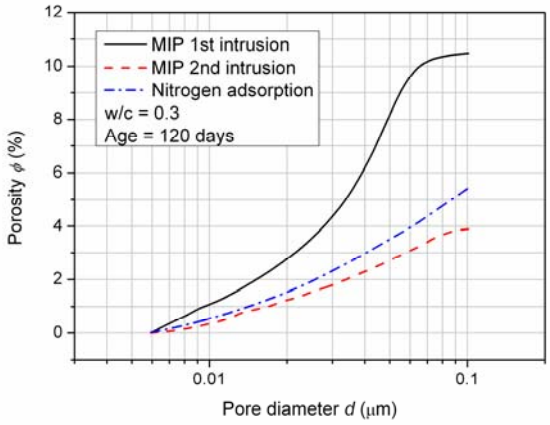

Fig. 8 Comparison of MIP and nitrogen adsorption results

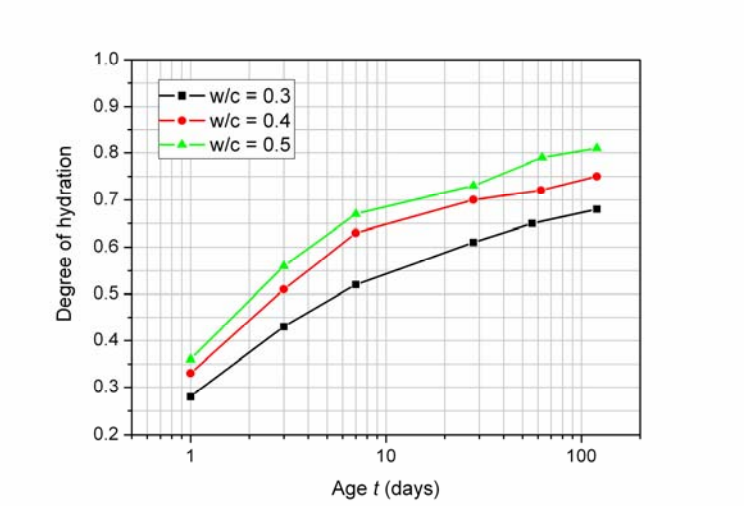

Fig. 9 Evolution of the degree of hydration determined by TGA

be proved by the vast resource of BSE images, the volume of ink-bottle pores should be dominated by large pores, and ink-bottle pores in the range of the throats as determined by MIP 2nd intrusion process should be limited. Thus the realistic pore size distribution curve should be between the two curves in Fig. 7(b), and much closer to the 2nd intrusion curve, in the range of less than the threshold pore diameter. This conclusion can be used as a criterion to judge whether a curve be realistic pore size distribution curve.

3.3.2 Comparison of pore size distribution curves from different techniques

As explained by Kaufmann *et al.* (2009), nitrogen adsorption detects pores from small ones to large ones, so ink-bottle effect does not influence this process but does influence the desorption process. Thus it can be expected that nitrogen adsorption is possible to generate much more realistic representation of the pore structure of cement based materials. After comprehensive comparisons of the results from MIP and nitrogen adsorption, this expectation has been confirmed by employing the above mentioned criterion. Results from the same sample as that in Fig. 7 are taken as an example for illustration (see Fig. 8). In Fig. 8, the porosity of pores in the mutual detectable range of MIP and nitrogen adsorption is re-cumulated from small size to large size. Obviously, the curve from nitrogen adsorption irrefragably lies between the MIP 1st and 2nd intrusion curves and much closer to the later, which proves that nitrogen adsorption does generate much more realistic representations of the pore structure of cement paste, compared with the conventional MIP technique.

3.4 Evolution of the degree of hydration

The simulation in the next section will be based on a status-oriented model. In this model, beside *w/c*, cement particle size distribution and the volume of small capillary pores determined by nitrogen adsorption, the degree of hydration is also an important input parameter. The evolution of degree of hydration of cement pastes with different *w/c*, determined by TGA, is plotted in Fig. 9. There is nothing special except normal regulations. The degree of hydration increases with time,

while the increasing rate is gradually lower. At each age, higher *w/c* results in higher degree of hydration. As shown in Fig. 9, only limited points have been determined by experiments, but interpolation can be employed to deduce the degree of hydration at any other age.

4. Numerical simulation

As aforementioned, MIP is incapable in providing valid pore size distribution of cement paste, while relatively, nitrogen adsorption generates much more realistic representation of the pore structure. However, pores in the range out of the measuring capacity of nitrogen adsorption need to be characterized by other method. In this study, the pores from several to 100 nm are defined as small capillary pores, and the ones larger than 100 nm as large capillary pores. Generally, two methods can be used for the characterization of large capillary pores, BSE imaging plus image analysis (Diamond 1989, Diamond and Leeman 1995, Lange *et al.* 1994, Scrivener 1989, Wang 1995) and numerical simulation plus image analysis (Ye 2003). The former needs complicated pre-treatment, and thus time-consuming. The later is relatively convenient, as once the algorithm and program are developed, all work can be performed by computer. The later method is adopted in the present study, and the former is employed to validate the simulation.

4.1 Algorithm

To simulate the hydration of cement and understand this process better, several computer based models have been developed since 1980s (Bentz 1997, Jennings and Johnson 1986, Maekawa *et al.* 1999, Navi and Pignat 1996, van Breugel 1991, Ye 2003). In these models, perhaps the HYMOSTRUC and CEMHYD3D are the most developed and active ones. HYMOSTRUC is a kinetics based computer model that was developed by van Breugel (1991) at TU Delft, the Netherlands, to simulate the reactions and microstructure in hydrating cement. It considers overall hydration kinetics, particle kinetics and particle interactions. In this model, the reaction products precipitate in the vicinity of the dissolving cement grains; both the dissolution and growth processes of the cement particles occur concentrically until particles contact each other. The cement particles of similar size hydrate at the same rate and their components react at equal fractional rates (Ye 2003). HYMOSTRUC can output microstructure following either time or the degree of hydration, considering the effects of *w/c*, cement particle size distribution, original cement composition and temperature. However, as the density of outer product layer is assumed constant throughout the hydration process and exclusive of any capillary pores, the pore structure simulated by HYMOSTRUC should be coarser than the realistic situation. CEMHYD3D is a digital-image based computer model proposed by Bentz and Garboczi in 1989 and developed in the last two decades at the National Institute of Standards and Technology (NIST, USA) (Bentz 1997, Ye 2003). In CEMHYD3D, after randomly distributing digitized spherical particles in a 3D computational volume following the particle size distribution of cement and *w/c*, particles are divided into 4 phases by a Box-Muller, an autocorrelation function and a rearrangement algorithm. Then, a cellular-automaton algorithm is applied to simulate the dissolution, diffusion, nucleation, precipitation, and contacting of cement constituents according to a set of probabilities (Bentz 1997). CEMHYD3D does not take hydration kinetics into account, so the microstructure is simulated following the degree of hydration, rather than time. CEMHYD3D has the advantage of considering all mineral components of cement, and due to the algorithm, it can easily deal with

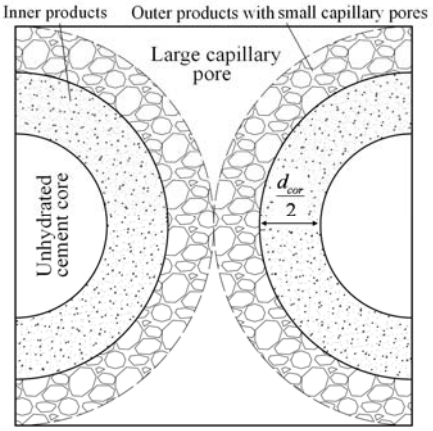

Fig. 10 Sketch of the assumptions of the model

non-spherical particles and the incorporation of mineral admixtures. However, the inner and outer products can not be distinguished from each other by this model, and problems exist in quantifying the pores (Ye 2003).

The newly developed model in this study is also based on the assumption of growing spheres (Jennings and Johnson 1986), just like HYMOSTRUC, but with some modifications. However, hydration kinetics is not considered in this model, and the microstructure is simulated against the degree of hydration. The generated microstructure-degree of hydration relationship can be translated to a microstructure-time relationship by applying specific hydration kinetics, if needed. The hydration of cement is governed by overall reaction stoichiometry, while in this paper, the classical Powers' model is adopted.

The initial unhydrated cement paste is simulated by randomly distributing spheres in a cubic REV (representative elementary volume) with periodic boundary conditions, according to cement particle size distribution measured in advance and *w/c*. This operation is conducted following a typical random sequential addition procedure as defined by Stroeven *et al.* (2009). Each particle is corroded inward to simulate the growth of inner products, and expanded outward to simulate the growth of outer products, as shown in Fig. 10. For a specific *w/c*, inputting a degree of hydration, a corresponding microstructure is obtained, without considering hydration kinetics. Thus this model is called a status-oriented model. Another important characteristic of this model is that small capillary pores determined by nitrogen adsorption are considered in simulation. As shown in Fig. 10, the inner products layer is assumed to be condensed (without capillary pore), while the outer products layer is not condensed due to the insufficient packing of hydrates in the sufficient space. To simplify the simulation, the volume of small capillary pores is added to the outer hydrates layer, and large capillary pores are simulated by the remained spaces out of the outer hydrates layer.

In this model, the degree of hydration (α) is defined as the volume fraction of hydrated cement, say, α equals to the volume of hydrated cement ($V_{hydrated}$) over the original cement volume (V_{cem})

$$\alpha = \frac{V_{hydrated}}{V_{cem}} \tag{6}$$

Assume that all cement particles are spheres with diameters from d_1 to d_n, and in hydration process, the spheres are corroded at the same rate in depth/step. Given a degree of hydration, some small spheres with diameter smaller than a critical value, d_{cor}, have been totally corroded while larger ones not. Thus

$$V_{hydrated} = \frac{1}{6}\pi\left(\sum_{d_1}^{d_{cor}} {d_i}^3 + \sum_{d_{cor+1}}^{d_n}\left({d_i}^3 - \left(d_i - d_{cor}\right)^3\right)\right) \tag{7}$$

$$V_{cem} = \frac{1}{6}\pi\sum_{d_1}^{d_n} {d_i}^3 \tag{8}$$

where d_{cor} is 2 times corroded depth as shown in Fig. 10. Hydrated cement changes to hydrates, and the volume expands by a factor κ_h, which represents the volume of hydrates created when a unit volume of cement is hydrated. According to Powers' model, κ_h approximates to 2.13 (Sanahuja *et al.* 2007). The original boundaries of cement particles are always there, in which and out of unhydrated cement core forms inner hydration products, and out of which outer hydrates deposit to form an outer products layer, with small capillary pores. All these descriptions are summarized as

$$V_{inner} = V_{hydrated} \tag{9}$$

$$V_{outer} = (\kappa_h - 1)\cdot V_{hydrated} \tag{10}$$

$$V_{outerlayer} = V_{outer} + V_{BJH} \tag{11}$$

$$V_{BJH} = \phi_{BJH}\cdot V_{REV} \tag{12}$$

where V_{inner} and V_{outer} indicate the volume of inner and outer products respectively; $V_{outerlayer}$ is the sum of the outer products volume and small capillary pore volume (V_{BJH}), which equals to the product of small capillary porosity determined by nitrogen adsorption and the volume of REV.

Giving a degree of hydration (α), through Eqs. (6) to (8), the parameter d_{cor} can be computed through a program. So far, each cement particle has an original boundary and an unhydrated core, whose diameter equals to the difference of the original diameter and d_{cor}. If the particle is smaller than or equals to d_{cor}, no unhydrated core exists. Besides, the outer layer expands outward from the original boundary step by step to mimic the total volume of outer layer determined by Eq. (11). Importantly, rules governing the growth of the outer layer need to be set. For this, most of researchers prefer to make outer products precipitate in the vicinity of the dissolving cement particle (Ye 2003). However, as stated by Taylor (1997), outer products can also precipitate on other grains. Thus in this model, all free surfaces exposed to the remained large pores are given the same opportunity to grow outward. When overlapping between growing spheres happens, only the

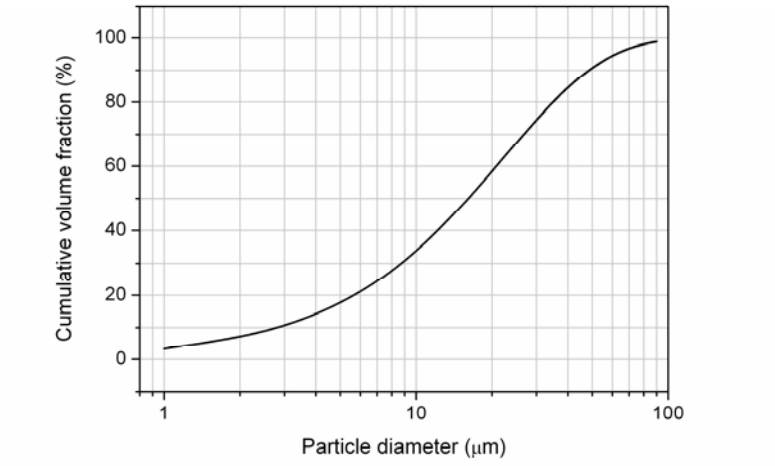

Fig. 11 Particle size distribution of cement used in simulation

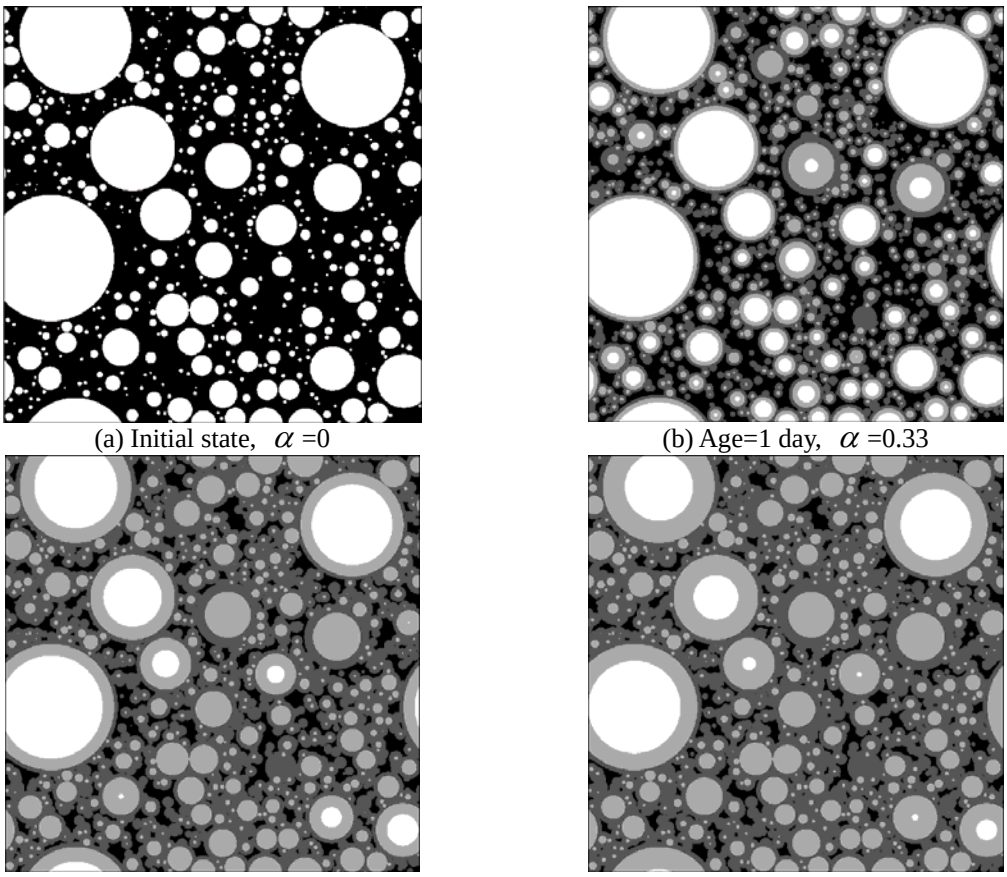

(a) Initial state, α =0 (b) Age=1 day, α =0.33

(c) Age=7 days, α =0.63 (d) Age=120 days, α =0.75

Fig. 12 Typical 2D images cut from the simulated 3D microstructure (*w/c*=0.4)

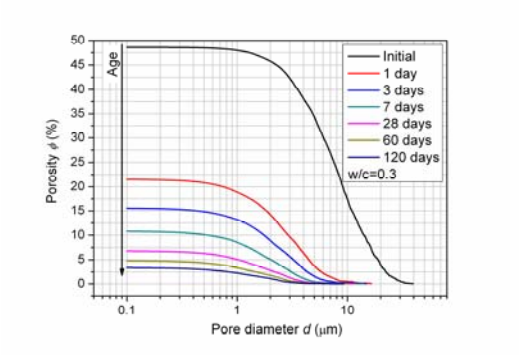

(a) *w/c*=0.3

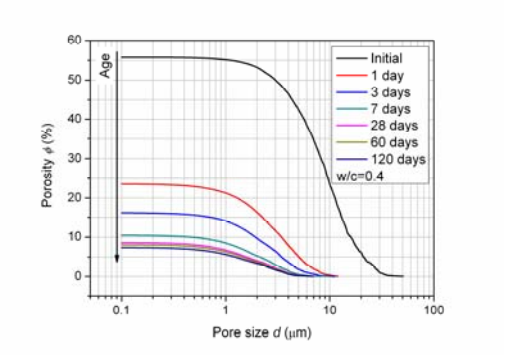

(b) *w/c*=0.4

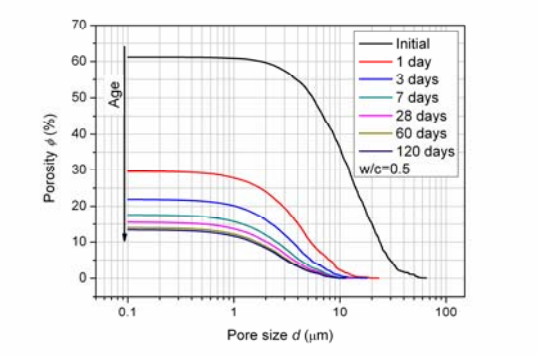

(c) *w/c*=0.5

Fig. 13 Pore size distribution curves deduced from the simulations

free surfaces are allowed to grow continuously along their out normal directs, in the same rate. Program ends once the volume of the outer layer equals to that calculated by Eq. (11).

At last, the simulated microstructure is digitized to an assemblage of voxels representing unhydrated cement cores, inner hydrates layers, outer hydrates layers and large capillary pores respectively. Two-dimensional (2D) images can be obtained from the simulated three-dimensional (3D) microstructure for pore structure analysis.

4.2 Simulation results

Cement pastes having the same conditions as those in the experimental studies are simulated by the newly developed model. A $100\times100\times100$ μm^3 cube is selected as the REV, and 1 micron (diameter) is selected as the minimum particle size of cement in the simulation, considering the balance between computer power and simulation accuracy. The particle size distribution of cement used for simulation is shown in Fig. 11. Another input factor, the degree of hydration is picked up from Fig. 9.

Fig. 12 shows the typical 2D images cut from the simulated 3D microstructure, in which colors white, light gray, dark gray and dark represent unhydrated cement core, inner hydrates layer, outer hydrates layer and large capillary pore, respectively. The examples are from the simulated pastes with *w/c*=0.4 at different ages (or degree of hydration). The evolution of the microstructure

following the degree of hydration can be clearly observed. Based on the simulated 3D microstructures, as suggested by Ye (2003), more than 12 sample 2D images are randomly cut, and analyzed to generate the pore size distribution curve of a cement paste at a specific status, through averaging. The comprehensive results are shown in Fig. 13. Note that in the digitization process, the pixel size selected is 0.1×0.1 μm^2, thus, as what can be directly seen from Fig. 13, only large capillary pores down to this limit can be involved in the pore size distribution curves. One can conveniently compare these results with those of MIP in Fig. 1.

4.3 Validation

Any numerical simulation needs to be validated theoretically or experimentally. In this study, BSE imaging plus image analysis is employed to validate the newly developed model in modeling the pore structure. For this purpose, cement pastes with *w/c*=0.4 and 0.5 at the age of 60 days were

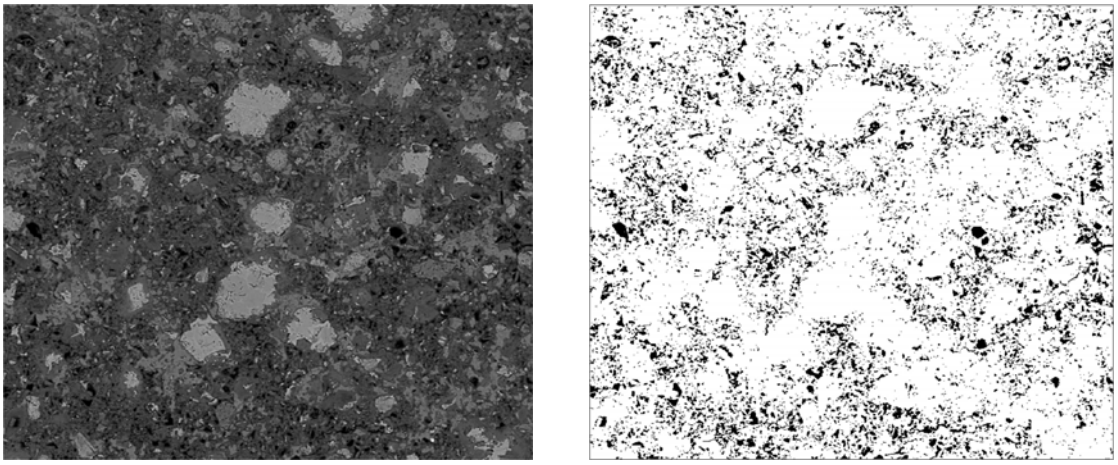

(a) Original image (b) Pore segmentation by binary processing

Fig. 14 A typical BSE image (*w/c*=0.5, age=60 days, 500×)

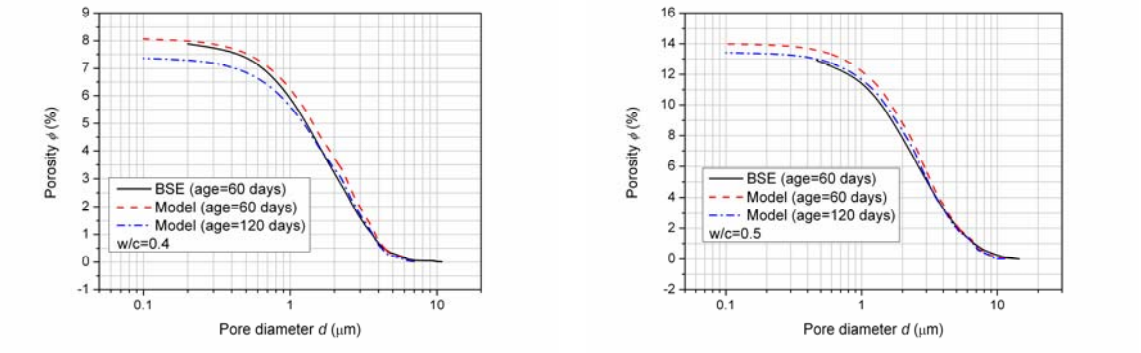

(a) *w/c*=0.4 (b) *w/c*=0.5

Fig. 15 Comparison of the pore size distribution curves from BSE image analysis and simulation (model)

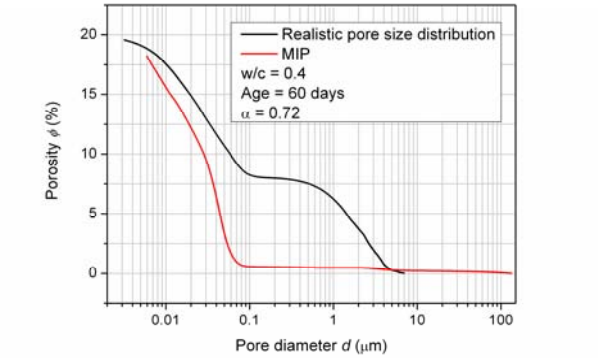

Fig. 16 Comparison of the realistic and MIP pore size distribution curves

the pore structure. For this purpose, cement pastes with *w/c*=0.4 and 0.5 at the age of 60 days were prepared to get images through BSE. A typical image is shown in Fig. 14(a).

It is well-known that, in BSE image analysis, the selection of threshold gray level for pore segmentation is the most important link, and selection by hand should be avoided. In this study, the method developed by Wong *et al.* (2006) is employed for pore segmentation, and the processed image is shown in Fig. 14(b). After pore segmentation, image analysis can be carried out to generate the pore size distribution curves. In Fig. 15, the results from numerical simulations are compared with those from BSE image analysis. It can be seen that, for both cement pastes, results from different techniques agree well with each other, which proves the validity of the newly developed model with relatively high accuracy in modeling the pore structure of cement pastes.

5. Realistic pore structure

For the better understanding of the properties of cement pastes (or concretes), researchers have been working on establishing their pore structure for many years. As mentioned above, HYMOSTRUC and CEMHYD3D are two excellent works on this issue, and they have advantages in specific aspects and of course limitations. Another example is from the work of Aït-Mokhtar *et al.* (2002), who established the pore structure using random cylindrical tubes based on MIP results. Unfortunately, this kind of work may not give good accuracy as MIP results are so invalid. Actually, as the microstructure of cement paste exhibits features over a wide range of length scale, it is really difficult to represent the microstructure over all length scales using a computer model. However, depending on the nature of specific problem, there must be a most relevant level of microstructure or “the pertinent microstructure level” (Pignat *et al.* 2005). Taking permeability for instance, works (Mindess *et al.* 2003, Neville 1996, Xu *et al.* 2009) have made researchers believe that it is the capillary pore system, from several nanometers to tens or hundreds of micrometers, which governs the permeability of cement based materials. Thus pores in this range should be focused on in studies for solving permeability problems.

According to the results from experiments and simulations in this study, the volume of small capillary pores decreases while the volume of outer hydrates layer increases following the evolution of hydration degree, and the size of small capillary pores in all samples follow the same

distribution mode. Based on these findings, a hypothesis can be made: at earlier hydration stage, outer products generated from diffusion controlled processes form the primary skeleton of the outer hydrates layer; following the evolution of the degree of hydration, particles of outer products are continuously formed and packed in the outer products layer, which leads to the densification of this layer on one hand, and the expansion of it on the other. Thus, rather than assuming that the densities of hydrates layers remain constant throughout the hydration process in HYMOSTRUC, the authors prefer to believe that the density of the outer products layer increases continuously.

The realistic pore structure of cement paste should be represented based on all the experiments, simulations and the hypothesis. It is overviewed briefly in Fig. 10. Gel pores exist in C-S-H gel, and this is not explained in detail here. Capillary pores are classified into small capillary pores and large capillary pores. The two kinds of capillary pores are both the remained spaces originally occupied by water. They are different in refinement mechanism. Spaces due to insufficient packing of hydrates in the outer products layer are small capillary pores, and spaces left out of the outer products layer are large capillary pores. If the large capillary pores can percolate through the whole material, high permeability can be expected; if not, and they can only be connected through outer product layers (or small capillary pores), permeability should be low. If small capillary pores are even disconnected, then a dramatically low permeability material is produced. From this idea, discretization methods can be employed to solve permeability and even diffusivity problems, combined with the 3D microstructure developed in this study.

The pore size distribution curve of a typical cement paste, combining the results from nitrogen adsorption and simulation, is re-plotted in Fig. 16 as an intuitive illustration of the realistic pore structure. This complete curve is called the realistic pore size distribution curve (temporarily limited to capillary pores). Comparing it with the corresponding MIP pore size distribution curve, the limitation of the later is clearly shown. Besides, because the smallest capillary pores and some large pores separated by the smallest capillary pores can not be detected by MIP, MIP gives more or less lower total porosity. In the computer model, large capillary pores are simulated by the spaces refined by overlapped spheres (hydrated cement particles), and all crystalline hydrates are assumed to be embedded in the hydration product layers rather than to nucleate and grow in open capillary space. This simplification may lead to the missing of a large part of pores from one to several times of pixel size on the simulated images and thus slightly coarser pore structure. That is why an obvious turning point appears at the joining point of the pore size distribution curves of small capillary pore and large capillary pore, as shown in Fig. 16. Further development of the computer model will build in algorithms to deal with the nucleation and growth of crystal hydrates phases, which will make the pore structure of the simulated large capillary space finer, and may further improve the continuity and smoothness of the realistic pore size distribution curve.

6. Conclusions

Through the present study, several conclusions can be drawn:

(1) Although MIP has been the most popular method for pore structure characterization, its limitations lead to lower estimation of the total porosity and much finer estimation of the pore size distribution of cement based materials.

(2) Nitrogen adsorption gives realistic representation of the pore structure in the range of pore size from 3 nm to 100 nm. Capillary pores in this range are named as small capillary pores. Small capillary pores in all samples follow the same distribution mode.

(3) A new status-oriented computer model has been developed to model the microstructure as a function of *w/c*, cement particle size distribution and the degree of hydration. 2D images can be obtained from the modeled microstructure for pore structure characterization. And the model has been validated by BSE imaging plus image analysis.
(4) Realistic pore structure of cement paste has been established by combining results of nitrogen adsorption and simulation by the newly developed status-oriented computer model.

Acknowledgements

The financial supports from China Basic Research Grant, Basic Research on Environmentally Friendly Contemporary Concrete (2009CB623200) and from National Natural Science Foundation of China under key project (50838008) are greatly acknowledged.

References

Aït-Mokhtar, A., Amiri, O., Dumargue, P. and Sammartino, S. (2002), "A new model to calculate water permeability of cement-based materials from MIP results", *Adv. Cem. Res.*, **14**(2), 43-49.
Aligizaki, K.K. (2006), *Pore structure of cement-based materials: Testing, interpretation and requirements*, Taylor & Francis, New York, U.S.A.
Barrett, E.P., Joyner, L.G. and Halenda, P.P. (1951), "The determination of pore volume and area distributions in porous substances: I. computations from nitrogen isotherms", *J. Am. Chem. Soc.*, **73**(1), 373-380.
Bentz, D.P. (1997), "Three-dimensional computer simulation of portland cement hydration and microstructure development", *J. Am. Ceram. Soc.*, **80**(1), 3-21.
Brandt, A.M. (2009), *Cement-based composites: Materials, mechanical properties, and performance (2nd ed.)*, Routledge, London, U.K.
CEB (Comité euro-international du béton) (1991), *Durable concrete structures: Design guide*, Thomas Telford, London, U.K.
Cook, R.A. and Hover, K.C. (1991), "Experiments on the contact angle between mercury and hardened cement paste", *Cement Concrete Res.*, **21**(6), 1165-1175.
Cook, R.A. and Hover, K.C. (1999), "Mercury porosimetry of hardened cement pastes", *Cement Concrete Res.*, **29**(6), 933-943.
Diamond, S. (2000), "Mercury porosimetry - an inappropriate method for the measurement of pore size distributions in cement-based materials", *Cement Concrete Res.,* **30**(10), 1517-1525.
Diamond, S. and Leeman, M.E. (1995), "Pore size distributions in hardened cement paste by SEM image analysis", *Mater. Res. Soc. Symposium Proceedings, 370, Microstructure of Cement-Based Systems/Bonding and Interfaced in Cementitious Materials*, 217-226.
Gallé, C. (2001), "Effect of drying on cement-based materials pore structure as identified by mercury intrusion porosimetry: A comparative study between oven-, vacuum-, and freeze-drying", *Cement Concrete Res.*, **31**(10), 1467-1477.
Gerhardt, R. (1989), "A review of conventional and non-conventional pore characterization techniques", *Mater. Res. Soc. Symposium Proceedings, 137, Pore Structure and Permeability of Cementitious Materials,* 75-82.
Gonzalez, R.C. and Woods, R.E. (2002), *Digital image processing (2nd ed.)*, Prentice Hall, Upper Saddle River, N.J., U.S.A.
Jennings, H.M. and Johnson, S.K. (1986), "Simulation of microstructure development during the hydration of a cement compound", *J. Am. Ceram. Soc.*, **69**(11), 790-795.

Kaufmann, J., Loser, R. and Leemann, A. (2009), "Analysis of cement-bonded materials by multi-cycle mercury intrusion and nitrogen sorption", *J. Colloid Interf. Sci.*, **336**(2), 730-737.
Lange, D.A., Jennings, H.M. and Shah, S.P. (1994), "Image-analysis techniques for characterization of pore structure of cement-based materials", *Cement Concrete Res.*, **24**(5), 841-853.
León, C.A.L.Y. (1998), "New perspectives in mercury porosimetry", *Adv. Colloid Interfac.*, **76-77**(1), 341-372.
Maekawa, K., Chaube, R. and Kishi, T. (1999), *Modelling of concrete performance: Hydration, microstructure formation, and mass transport*, Routledge, New York.
Miller, M., Bobko, C., Vandamme, M. and Ulm, F.J. (2008), "Surface roughness criteria for cement paste nanoindentation", *Cement Concrete Res.*, **38**(4), 467-476.
Mindess, S., Darwin, D. and Young, J.F. (2003), *Concrete (2nd ed.)*, Prentice Hall, Upper Saddle River, N.J., U.S.A.
Moro, F. and Böhni, H. (2002), "Ink-bottle effect in mercury intrusion porosimetry of cement-based materials", *J. Colloid Interf. Sci.*, **246**(1), 135-149.
Navi, P. and Pignat, C. (1996), "Simulation of cement hydration and the connectivity of the capillary pore space", *Adv. Cement Based Mater.*, **4**(2), 58-67.
Neville, A.M. (1996), *Properties of concrete (4th a final ed.)*, J. Wiley, New York.
Pignat, C., Navi, P. and Scrivener, K. (2005), "Simulation of cement paste microstructure hydration, pore space characterization and permeability determination", *Mater. Struct.*, **38**(5), 459-466.
Sanahuja, J., Dormieux, L. and Chanvillard, G. (2007), "Modelling elasticity of a hydrating cement paste", *Cement Concrete Res.*, **37**(10), 1427-1439.
Scrivener, K.L. (1989), "The use of backscattered electron microscopy and image analysis to study the porosity of cement paste", *Mater. Res. Soc. Symp. Proceedings,* 137*, Pore Structure and Permeability of Cementitious Materials,* 129-140.
Stroeven, P., Hu, J. and Stroeven, M. (2009), "On the usefulness of discrete element computer modeling of particle packing for material characterization in concrete technology", *Comput. Concrete*, **6**(2), 133-153.
Tang, C. (2010), "Hydration properties of cement pastes containing high-volume mineral admixtures", *Comput. Concrete*, **7**(1), 17-38.
Taylor, H.F.W. (1997), *Cement chemistry (2nd ed.)*, T. Telford, London.
van Breugel, K. (1991), *Simulation of hydration and formation of structure in hardening cement-based materials*, Doctoral dissertation, Delft University of Technology, Delft, the Netherlands.
Wang, Y.T. (1995), *Microstructural study of hardened cement paste by backscatter scanning electron microscopy and image analysis*, Doctoral dissertation, Purdue University, West Lafayette, IN., U.S.A.
Webb, P., Orr, C. and Micromeritics Instrument Corporation. (1997), *Analytical methods in fine particle technology*, Micromeritics Instrument Corporation, Norcross, GA., U.S.A.
Winslow, D.N. and Diamond, S. (1970), "A mercury porosimetry study of the evolution of porosity in Portland cement", *J. Mater.*, **5**(3), 564-585.
Wong, H.S. , Head, M.K. and Buenfelda, N.R. (2006), "Pore segmentation of cement-based materials from backscattered electron images", *Cement Concrete Res.*, **36**(6), 1083-1090.
Xu, S., Simmons, G.C., Mahadevan, T.S., Scherer, G.W., Garofalini, S.H. and Pacheco, C. (2009), "Transport of water in small pores", *Langmuir*, **25**(9), 5084-5090.
Ye, G. (2003), *Experimental study and numerical simulation of the development of the microstructure and permeability of cementitious materials*, Doctoral dissertation, Delft University of Technology, Delft, the Netherlands.
Young, J.F., Mindess, S., Bentur, A. and Gray, R.J. (1998), *The science and technology of civil engineering materials*, Prentice Hall, Upper Saddle River, N.J., U.S.A.
Zhang, J. (2008), *Microstructure study of cementitious materials using resistivity measurement*, Doctoral dissertation, The Hong Kong University of Science and Technology, Hong Kong, China.